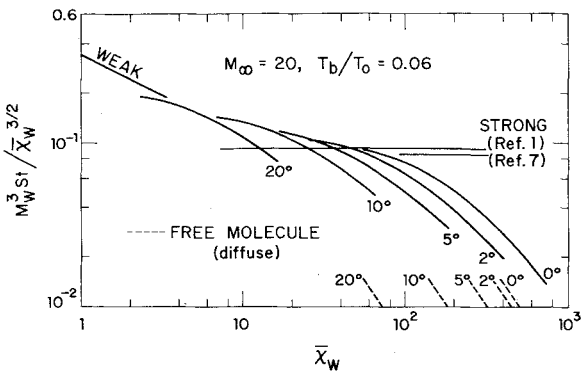

Fig. 4 Wedge heat transfer rate on equivalent flat plate basis.

and

$$\frac{(M^3St/\bar{\chi}^{3/2})_w}{(M^3St/\bar{\chi}^{3/2})_\infty} = \left[\frac{M_w}{M_\infty}\left(\frac{\bar{\chi}_\infty}{\bar{\chi}_w}\right)^{1/2}\right]^3 \frac{(\rho u)_w}{(\rho u)_\infty} \tag{4}$$

in which $(\ )_w$ implies the use of inviscid conditions downstream of an oblique shock of turning angle θ_b, and $St_\infty = -\dot{q}_b/(\rho u)_\infty(h_o - h_b)$ is the non-dimensional heat transfer flux. Application of Eqs. (3) and (4) to the exact solutions and experimental data of Figs. 1 and 2, and introducing $(p_b)_{\text{inviscid}}$ as the pressure datum, yields the equivalent plate results for each wedge angle (Figs. 3 and 4; $\theta_b = 10°$ and 20° loci are dashed for clearness in Fig. 3). The experimental data in Fig. 3 were plotted from the original source,[5] which indicated a smooth decay to the inviscid wedge limit. The plate ($\theta_b = 0°$) solution is from Ref. 2.

In this form, the merged solutions are seen to be initiated at appreciably decreasing $\bar{\chi}_w$ as shock strength (i.e., θ_b) increases. The peak pressure interaction proves to be much weaker for thicker wedges. The experimental points confirm the theoretical trends (as expected in view of Figs. 1 and 2) but clearly extend into the weak interaction region and provide no evidence of a "negative" interaction. The portion of the $\theta_b = 20°$ curve for $(p_b)/(p_b)_{\text{inviscid}} < 1$ and the implied extrapolation of at least the 10° curves suggest a failure of Shorenstein's method[3] at sufficiently small $\bar{\chi}_w$. Nevertheless, the larger θ_b solutions do properly approximate the data band in the transition between the strong and weak regimes. The experimental points have been omitted from Fig. 4 for clarity but again are comparably clustered along the exact solutions as in Fig. 2.

In general, smaller interaction effects were to be expected for wedges in contrast to a plate as a result of the strong inviscid pressure field.[7] Effectively, the lesser $\bar{\chi}_w$ (e.g., $\bar{\chi}_w/\bar{\chi}_\infty \cong 0.1$ for $\theta_b = 10°$) contracts the (dimensional) distance within which the interaction is important. In addition, however, Figs. 3 and 4 illustrate the weakening that results from the merging process for stronger shocks. It is clear that for large wedge angles ($\theta_b \approx 20°$) the strong regime is virtually eliminated.

References

[1] Pan, Y. S. and Probstein, R. F., "Rarefied Flow Transition at a Leading Edge," *Fundamental Phenomena in Hypersonic Flow*, Cornell University Press, Ithaca, N.Y., 1966, pp. 259–306.

[2] Shorenstein, M. L. and Probstein, R. F., "The Hypersonic Leading Edge Problem," *AIAA Journal*, Vol. 6, No. 10, Oct. 1968, pp. 1898–1906.

[3] Shorenstein, M. L., "Hypersonic Leading Edge Problem: Wedges and Cones," *AIAA Journal*, Vol. 10, No. 9, Sept. 1972, pp. 1173–1179.

[4] Shorenstein, M. L., "A Hypersonic Merged Layer Model for Sharp Wedges and Cones," Ph.D. thesis, Dept. of Aeronautics and Astronautics, MIT, Cambridge, Mass., Jan. 1971.

[5] Vidal, R. J. and Bartz, J. A., "Surface Measurements on Sharp Flat Plates and Wedges in Low-Density Hypersonic Flow," *AIAA Journal*, Vol. 7, No. 6, June 1969, pp. 1099–1109.

[6] Tannehill, J. C., Mohling, R. A. and Rakich, J. V., "Numerical Computation of Hypersonic Viscous Flow over a Sharp Leading Edge," *AIAA Journal*, Vol. 12, No. 2, Feb. 1974 pp. 129–130.

[7] Hayes, W. D. and Probstein, R. F., *Hypersonic Flow Theory*, Academic Press, New York, 1959.

Model for the Solution of Supersonic Viscous Interaction Effects on Blunted Cones

GABRIEL MILLER* AND ANDREW SROKOWSKI†
New York University, New York, N.Y.

Introduction

THE problem area of low density, supersonic and hypersonic flows over blunted cones has received much theoretical[1–5] and experimental,[6–12] attention over the past decade. The practical application of such investigations: space vehicle re-entry and high altitude flight, has initiated the development of numerous analytical and numerical models to accurately predict the viscous inviscid interaction and its effect on fluid properties, particularly pressure distribution.

A proper assessment of the effects of interaction on blunted surfaces can only be accomplished by a theory which allows for both pressure and vorticity interaction phenomena for the high Mach number, low Reynolds number flows of practical interest. Previous investigations by the authors[13,14] have attempted to establish a model which allows for the inclusion of all interaction effects directly, i.e., by solving the entire viscous and inviscid flowfield at the same time and establishing unique solutions. The model's main features are: its inclusion of viscous transports in the characteristic equations, the matching of the subsonic viscous flow (solved by a second-order, implicit Crank-Nicholson scheme) to the supersonic flow in the transonic zone, the inclusion of the normal momentum equation (thus allowing for transverse pressure gradients, whose importance is increased in thick, high curvature boundary layers), and the solution of the entire interaction problem by a marching technique. It is shown herein that the model's predictions of pressure distribution and heat transfer for high Mach number, low Reynolds number, flows over blunted cones are in excellent agreement with experimental data, whereas other interaction models do not exhibit such accuracy.

Method of Analysis

The calculation of the flowfield is divided into three parts; 1) the subsonic boundary layer, 2) the supersonic region (including viscous transports), and 3) the matching region.

1) Subsonic boundary layer

The equations for the inner, highly viscous, region are represented by the boundary-layer equations in coordinates measured along and normal to the body. Consistent with the hypothesis of moderate Reynolds number, terms of order $[1/(Re_\infty)^{1/2}]$ are retained after coordinate stretching. As normal pressure gradients are impressed on the inner region from the outer (supersonic) flow, and since body curvature may be significant, the normal momentum equation is retained. Thus, for axisymmetric flowfields, the equations are[13,14]

$$(R\rho u)_{\bar{x}} + (\beta R\rho\bar{v})_{\bar{y}} = 0$$

$$\rho[uu_{\bar{x}} + \beta\bar{v}u_{\bar{y}} + \kappa u\bar{v}/(Re_\infty)^{1/2}] + p_{\bar{x}} = S_1'$$

$$\rho[u\bar{v}_{\bar{x}}/(Re_\infty)^{1/2} + \beta\bar{v}\bar{v}_{\bar{y}}/(Re_\infty)^{1/2} - \kappa u^2] + \beta p_{\bar{y}}(Re_\infty)^{1/2} = 0$$

$$\rho(uT_{\bar{x}} + \beta\bar{v}T_{\bar{y}}) - E_\infty(up_{\bar{x}} + \beta\bar{v}p_{\bar{y}}) = S_2'$$

Received July 25, 1974. This work was supported by the Department of the Navy, Office of Naval Research, under Contract N00014-67-A-0467-0021.

Index category: Subsonic and Transonic Flow.

* Associate Professor of Applied Science, New York University.

† Associate Research Scientist, Aerospace Laboratory; presently Engineering Technologist, NASA Langley Research Center, Hampton, Va.

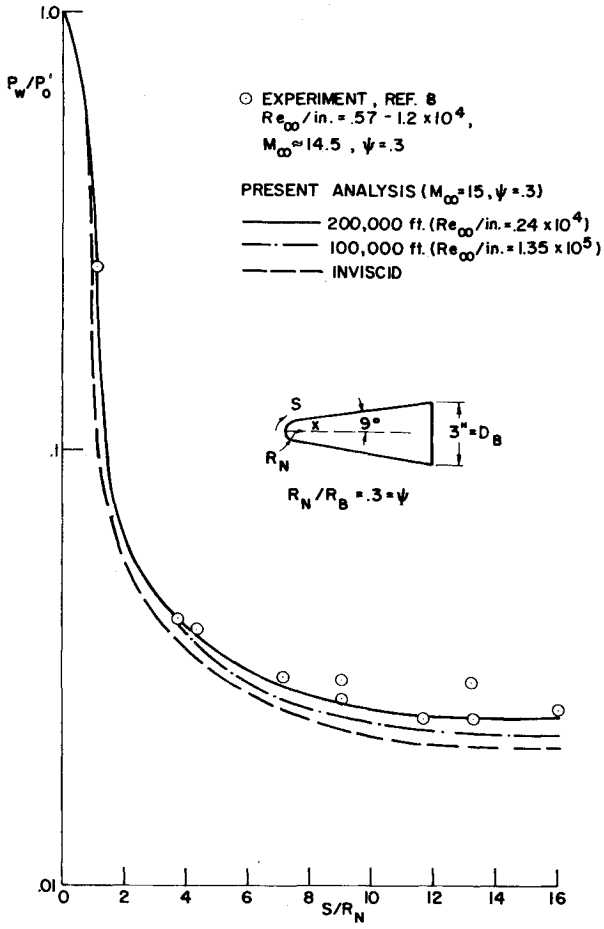

Fig. 1 Pressure distribution on blunted cone as function of altitude.

where

$$S_1' = \beta\left[(\bar{\mu}u_{\bar{y}})_{\bar{y}} - \kappa\frac{(\mu u)_{\bar{y}}}{(Re_\infty)^{1/2}} + \bar{\mu}\left(2\kappa + \frac{\cos\theta}{R}\right)\frac{u_{\bar{y}}}{(Re_\infty)^{1/2}}\right]$$

$$S_2' = \beta\left[\frac{1}{Pr}(\bar{\mu}T_{\bar{y}})_{\bar{y}} + \frac{1}{Pr}\left(\kappa + \frac{\cos\theta}{R}\right)\frac{\bar{\mu}T_{\bar{y}}}{(Re_\infty)^{1/2}} + E_\infty\bar{\mu}(u_{\bar{y}})^2 - 2\kappa\bar{\mu}E_\infty\frac{uu_{\bar{y}}}{(Re_\infty)^{1/2}}\right]$$

2) Supersonic region

In the supersonic region, viscous transports normal to streamlines are retained in the characteristic net, thus yielding the following characteristic relations:

$$\frac{dP}{\gamma P} \pm \frac{d\theta}{\sin\mu\cos\mu} + \left[\frac{\sin\theta}{R} + \frac{S_1}{\rho q^2} - \frac{(\gamma-1)S_2}{\gamma pq}\right]\times \frac{dx}{\cos\mu\cos(\theta\pm\mu)} = 0$$

along

$$dy/dx = \tan(\theta\pm\mu)$$

where

$$S_1 = \frac{1}{Re_\infty}\left[\frac{\partial}{\partial n}\left(\bar{\mu}\frac{\partial q}{\partial n}\right) + \frac{\cos\theta}{y}\bar{\mu}\frac{\partial q}{\partial n}\right]$$

$$S_2 = \frac{1}{Re_\infty}\left[\bar{\mu}\left(\frac{\partial q}{\partial n}\right)^2 + \left\{\frac{\partial}{\partial n}\left(k\frac{\partial T}{\partial n}\right) + \frac{\cos\theta}{y}k\frac{\partial T}{\partial n}\right\}\Big/ Pr\,E_\infty\right]$$

Since viscous transports are included in the characteristic net, the mass flow—entropy table (which is used to determine flow properties) must be remade at each step as entropy along streamlines is no longer conserved. The bow shock calculation includes the effects of viscous transports, consistent with the inclusion of second-order effects. The equations for the calculation are presented extensively in Ref. 13.

3) Matching of supersonic and subsonic flow

The basic marching procedure is accomplished by first guessing the streamline deflection at the matching point of a station $\Delta\bar{x}$ downstream (the distance being dictated by the characteristic intersection length at the matching point). The characteristic relation determines the pressure and thus all data at the top of the subsonic zone is known. From the matrix inversion, the inner flowfield is calculated. The inner profiles are then utilized to determine the value of the stream function at the surface. If the stream function at the wall $\neq 0$, a new value of streamline deflection is guessed until convergence (at most, four or five iterations are required).

In order to initiate the interaction analysis for flows around blunt bodies, flow profiles must be known along a line normal to the surface at some point past the sonic line. The inviscid flowfield about the blunt nose is accomplished using the program of Ref. 15. A standard boundary-layer analysis then determines the viscous profiles. A smooth composite initial profile is then produced[13] utilizing inner-outer expansion theory. This method is consistent with the interaction analysis since interaction effects would not be dominant in the zone upstream of the sonic line.

Results and Conclusions

The flow model was applied to a 9° half angle cone with nose radius of 0.45 in., base radius of 1.5 in. and length of 7 in. in a Mach 15 flow. The wall temperature was chosen equal to one tenth the freestream stagnation value. Two Reynolds numbers were studied for comparison to experimental data, the first 1.35×10^5 per in. (corresponding to a flight altitude of 100,000 ft) and the second 0.24×10^4 per in. (corresponding to a flight altitude of 200,000 ft).

Figure 1 shows the ratio of wall pressure to stagnation pressure along the surface. The influence of interaction is readily apparent and its effect pronounced. On the spherical cap, the

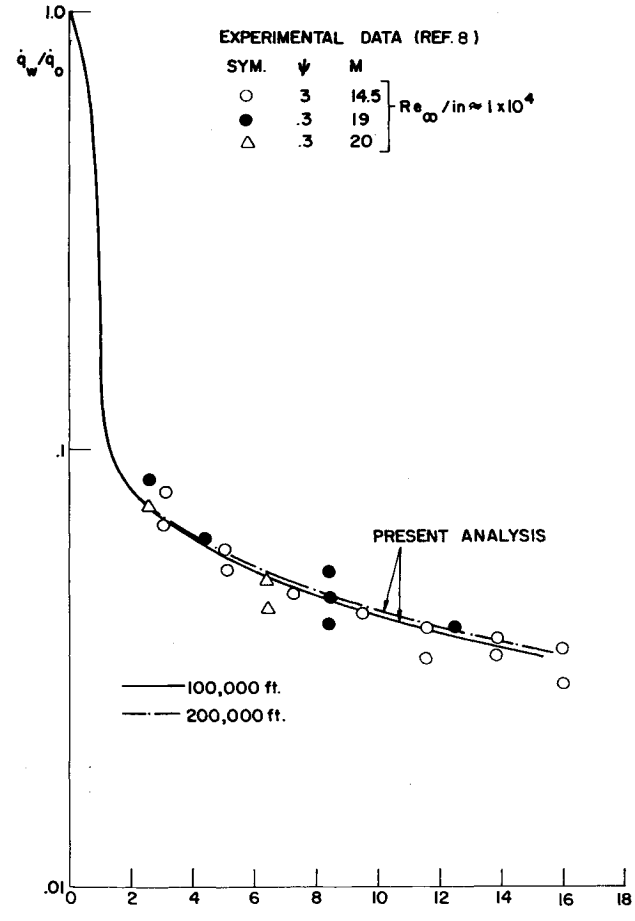

Fig. 2 Heat transfer distribution on blunted cone.

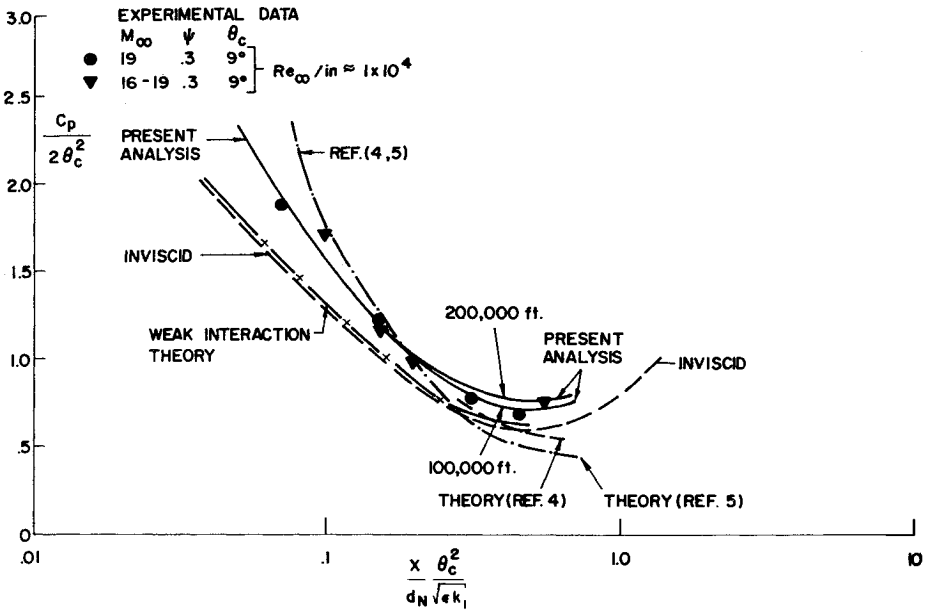

Fig. 3 Pressure distribution in correlation variables.

effects of curvature led to normal pressure gradients on the order of 35%, thus indicating the importance of the inclusion of the normal momentum equation for low Reynolds number flows over highly curved surfaces. The results are compared to an experimental case[8] whose Mach and Reynolds numbers correspond closely to the 200,000 ft run. The agreement between the high altitude curve and the data is quite good. Figure 2 shows the ratio of wall to stagnation point heat transfer rates along the surface. As expected (and as indicated by the data) the effect of interaction has a much smaller effect on heat transfer rate.

Figure 3 presents the surface pressure coefficient in terms of Cheng's[5] correlation parameters for the altitudes (or Reynolds numbers) computed by the model. The effects of Reynolds number are somewhat compressed in terms of the parameters. The results are in good agreement with experimental data which are in the Reynolds number range between the two cases run. The blast wave theory prediction of Chernyi[4] and the zeroth-order theory of Cheng[5] first overpredict and then underpredict the pressure distribution, while the inviscid distribution and the perturbation due to weak interaction theory underpredict the curve throughout. In the altitude range considered an increase in the drag coefficient of as much as 20% can be expected due to the interaction effects. Figure 4 presents the wall heat transfer rates predicted by the model in terms of the modified Cheng heat transfer correlation parameters. The prediction is in good agreement with a variety of experimental data.

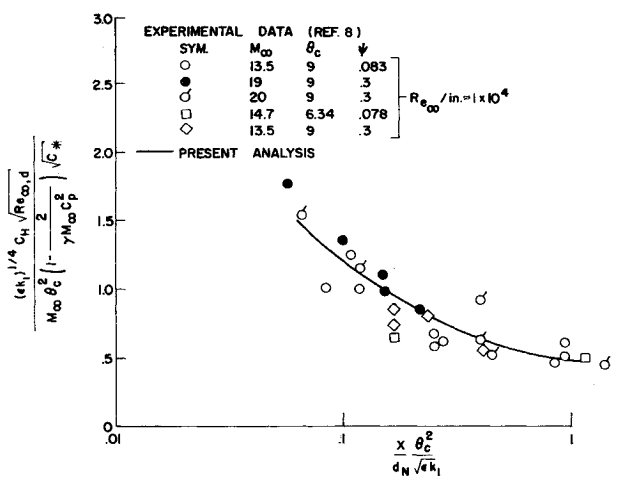

Fig. 4 Heat transfer distribution in correlation variables.

In conclusion, the predictions of the analytical and numerical model give excellent quantitative results for flows over blunted cones in hypersonic flight at high altitudes. The correct determination of the aerodynamic performance of a vehicle at high altitudes requires an analysis of this type in order to quantitatively predict the pressure distribution within reasonable accuracy.

References

[1] Lees, L., "Laminar Heat Transfer Over Blunt-Nosed Bodies at Hypersonic Flight Speeds," *Jet Propulsion*, Vol. 26, April 1956, pp. 259–260.

[2] Davis, R. T. and Flugge-Lotz, I., "Second-Order Boundary-Layer Effects in Hypersonic Flow Past Axisymmetric Blunt Bodies," *Journal of Fluid Mechanics*, Vol. 20, Pt. 4, 1964, pp. 593–623.

[3] Stewartson, K., "Viscous Hypersonic Flow Past a Slender Cone," *Physics of Fluids*, Vol. 7, 1964, pp. 667–675.

[4] Chernyi, G. G., "Flow around a Thin Blunt Cone at High Supersonic Speeds," *Proceedings of Academy of Sciences, USSR*, Vol. 112–117, 1957, pp. 263–266.

[5] Cheng, H. K., et al., "Boundary-Layer Displacement and Leading Edge Bluntness Effects in High Temperature Hypersonic Flow," *Journal of Aerospace Sciences*, Vol. 28, 1961, pp. 353–382.

[6] Lewis, C. H., "Pressure Distribution and Shock Shape Over Blunted Slender Cones at Mach Numbers from 16 to 19," AEDC TN-61-81, 1961, Arnold Engineering Development Center, Tullahoma, Tenn.

[7] Roberts, J. F., Lewis, Clark, H., and Rud, M., "Ideal Gas Spherically Blunted Cone Flow Field Solutions at Hypersonic Conditions," AEDC-TR-66-121, Arnold Air Force Station, Tenn., Aug. 1966.

[8] Griffith, B. J. and Lewis, C. H., "Laminar Heat Transfer to Spherically Bluted Cones at Hypersonic Conditions," *AIAA Journal*, Vol. 2, No. 3, March 1964, pp. 438–444.

[9] Dayman, B. Jr., "Hypersonic Viscous Effects on Free-Flight Slender Cones," *AIAA Journal*, Vol. 3, No. 8, Aug. 1965, pp. 1391–1400.

[10] Whitfield, J. D. and Griffith, B. L., "Hypersonic Viscous Drag Effects on Blunt Slender Cones," *AIAA Journal*, Vol. 2, No. 10, Oct. 1964, pp. 1714–1722.

[11] Whitfield, J. D. and Griffith, B. J., "Viscous Drag Effects on Slendes Cones in Low-Density Hypersonic Flow," *AIAA Journal*, Vol. 3, No. 6, June 1965, pp. 1165–1166.

[12] Lochman, W. K., "Free-Flight Base Pressure and Heating Measurements on Sharp and Blunt Cones in a Shock Tunnel," *AIAA Journal*, Vol. 5, No. 10, Oct. 1967, pp. 1898–1899.

[13] Srokowski, A. and Miller, G., "A Method for the Analysis of Viscous Inviscid Interaction Effects on Blunt Bodies in Hypersonic Flight," NYU-AA-72-10, June 1972, New York University, New York.

[14] Miller, G., "The Mathematical Formulation of Viscous-Inviscid Interaction Problems in Supersonic Flow," *AIAA Journal*, Vol. 11, No. 7, July 1973, pp. 938–942.

[15] Lomax, H. and Inouye, M., "Numerical Analysis About Blunt Bodies Moving at Supersonic Speeds in an Equilibrium Gas," TR-204, July 1964, NASA.